

**HYDROGEOLOGIC STRUCTURE UNDERLYING A RECHARGE POND
DELINEATED WITH SHEAR-WAVE SEISMIC REFLECTION AND CONE
PENETROMETER DATA**

Seth S. Haines, U.S. Geological Survey, Denver, shaines@usgs.gov

Adam Pidlisecky, University of Calgary

Rosemary Knight, Stanford University

Submitted 8 October, 2008, to Near Surface Geophysics
for the EAGE/SEG special issue on Hydrogeophysics
Resubmitted 18 February, 2009

**HYDROGEOLOGIC STRUCTURE UNDERLYING A RECHARGE POND
DELINEATED WITH SHEAR-WAVE SEISMIC REFLECTION AND CONE
PENETROMETER DATA**

Seth S. Haines, U.S. Geological Survey, Denver, shaines@usgs.gov

Adam Pidlisecky, University of Calgary

Rosemary Knight, Stanford University

ABSTRACT

With the goal of improving the understanding of the subsurface structure beneath the Harkins Slough recharge pond in Pajaro Valley, California (USA), we have undertaken a multimodal approach to develop a robust velocity model to yield an accurate seismic reflection section. Our shear-wave reflection section helps us identify and map an important and previously unknown flow barrier at depth; it also helps us map other relevant structure within the surficial aquifer. Development of an accurate velocity model is essential for depth conversion and interpretation of the reflection section. We incorporate information provided by shear-wave seismic methods along with cone penetrometer testing (CPT) and seismic CPT (SCPT) measurements. One velocity model is based on reflected and refracted arrivals and provides reliable velocity estimates for the full depth range of interest when anchored on interface depths determined from cone data and borehole drillers' logs. A second velocity model is based on SCPT data that provide higher-resolution 1D velocity columns with error estimates within the depth range of the CPT. Comparison of the reflection/refraction model with the SCPT model also suggests that the mass of the cone truck can influence

velocity with the equivalent effect of approximately one meter of extra overburden stress. Together, these velocity models and the depth-converted reflection section result in a better constrained hydrologic model of the subsurface and illustrate the pivotal role that cone data can provide in the reflection processing workflow.

INTRODUCTION

Over the past ten years there has been growing interest in the use of the subsurface for water storage. One type of system uses wells to inject and recover the water. A second type of system uses shallow ponds, either natural or excavated, for the infiltration of water into the subsurface and then uses wells to recover the water. The design and operation of these subsurface systems (e.g., Bouwer, 2002) require an understanding of the hydrogeologic structure and properties that control both the movement and storage of water.

In this case study, we worked at the Harkins Slough recharge pond in Pajaro Valley, California (USA). The operational model of the storage/recovery project involves filling the pond with water in the winter months to enable percolation into the surficial aquifer, and then recovering the water using wells around the pond for use in the summer months. On-going studies at the site are focused on answering fundamental questions similar to those posed in many hydrogeophysical studies, such as (1) what are the hydrogeologic controls on subsurface fluid flow?, and (2) what information can we glean from geophysical methods about the subsurface structure and properties that can be used to help populate and constrain hydrologic flow models?

Seismic reflection methods are a well-established means of determining near-surface structure (e.g., Hunter et al., 1984; Steeples and Miller, 1990; Brouwer and Helbig, 1998; Steeples and Miller, 1998). Shear wave methods (generally using horizontally polarized shear (SH) waves) have proven useful in near-surface studies (e.g., Helbig and Mesdag, 1982; Stumpel et al., 1984; Hasbrouck, 1991; Carr et al., 1998; Woolery et al., 1993; Pugin et al., 2004). Seismic velocity models are a necessary by-product of reflection data processing, essential to normal-moveout (NMO) correction and/or to migration velocity analysis (e.g., Yilmaz, 2001). Whether conducted as part of a depth migration scheme (e.g., Bradford et al., 2006) or independently (e.g., Baker, 1999), depth-conversion of seismic data is only as accurate as the velocity model that is used. When the subsurface is sufficiently simple, the velocity model from NMO velocity analysis can be adequate for depth conversion and other interpretation (Baker, 1999). Traveltimes of refracted arrivals can be used to develop other velocity models (e.g., Palmer, 1981; Zelt et al., 2006; Martí et al., 2008) and reflection arrival times can provide additional information (e.g., Stork and Clayton, 1991; Zelt and Smith 1992). It is well established that any velocity model will be more reliable if it is also based on supplemental information such as vertical-seismic profiling (VSP) results. Independent of reflection processing, velocity models can be used to infer structure (Zelt et al., 2006; Martí et al., 2008). Moreover, when combined with rock physics relations, velocity models can be used to infer material properties such as clay content or porosity.

Cone penetrometer testing (CPT) is widely used for engineering applications to

determine the properties of unconsolidated sediments (Campanella and Weemees, 1990; Daniel et. al., 1999). Ghose and Goudswaard (2004) presented an algorithm for calibrating SH-reflection-interpreted soil properties with cone tip measurement data. In addition some cones include an accelerometer that can be used for VSP measurements (Campanella and Robertson, 1984; Hunter et al., 2002). Jarvis and Knight (2002) demonstrated the value of quantitatively including seismic CPT (SCPT) data in the inversion and hydrogeologic interpretation of SH-wave reflection seismic data.

Our objective in this study was to obtain a shear-wave seismic reflection image incorporating CPT and SCPT data that would lead to improved understanding of the hydrogeologic structure controlling the operation of the Harkins Slough recharge pond. The key aspect that we focus on is obtaining and assessing a seismic velocity model to aid in processing and interpretation of our reflection section. Studies at the site are on-going and determination of large-scale structure is a critical step toward the development of a robust subsurface hydrogeologic model.

We begin by providing background hydrologic and geologic information on the Harkin Slough pond site, and discuss the data that we have available. We then present an SH-wave reflection section in the time domain, and review the available options for converting the section to depth. We present a set of velocity models, assessing the strengths and weaknesses of each, and then present our two preferred models and the corresponding depth-converted reflection sections. We conclude with an analysis of the velocity models available to us in this case study.

DESCRIPTION OF THE FIELD SITE

The Harkins Slough recharge pond is located approximately 5 km west of Watsonville, California and 1 km from the coast. This pond was designed and constructed by CH2M Hill and is managed by the Pajaro Valley Water Management Agency (PVWMA). It has been in operation since the fall of 2001. The pond is filled with water during the winter months (typically January to March); the water percolates through the base of the pond and is stored in an alluvial aquifer. Water is retrieved from recovery wells around the pond in the summer to reduce the groundwater needs (or to supplement the water supply) of the local farmers in this coastal zone. A key issue being addressed by PVWMA is the fact that, at the time of recovery, only 15% of percolated water remains in the capture zones of the recovery wells.

A schematic in Figure 1 is a simplified cross-section of the region beneath the pond. Drillers' logs from the 10 recovery wells around the pond report a thick continuous clay layer 35 to 50 m below ground surface. Above this clay layer are approximately 3 or more meters of interlayered sand and/or gravel locally with some silt and clay, overlain by approximately 30 m of sand. Cores recovered from depths to 7.5 m show the sand to be very clean. At or near the base of the sand layer, there are reports in some of the drillers' logs of thin units (1 to 2 m) of clay (referred to as sandy clay or lean clay) or clayey sand. It was presumed, in the design of the recharge pond, that these were isolated clay lenses or a discontinuous paleosol. The conceptual model for the operation of the pond is that the water is stored as a perched zone above the continuous lower clay layer; the recovery wells are screened just above this layer. At the time of

our surveys, the pond was dry and the measured hydraulic head was approximately 20 m below the ground surface in nearby wells. In Figure 2 we show an outline of the pond and the locations where we acquired seismic and CPT data.

DESCRIPTION OF THE CPT DATA

Cone penetrometer testing is a method that was developed by geotechnical engineers for obtaining high-resolution depth logs of mechanical soil properties without the need for boreholes (Campanella and Weemees, 1990; Daniel et. al., 1999). A cone penetrometer, commonly referred to as a cone, is a 36-mm-diameter steel rod, with sensors mounted close to a cone-shaped tip. The cone is pushed into unconsolidated materials using hydraulic rams mounted on a large truck, referred to as the cone truck. While the cone is being pushed, measurements are made with the sensors in the tip of the cone with a typical sampling interval of 5 cm. The standard cone penetrometer measures three separate ground properties: tip penetration resistance, friction sleeve resistance, and induced pore pressure, all of which are used to obtain information about subsurface stratigraphy. In addition to these standard CPT measurements, many cone penetrometers are equipped with a horizontal accelerometer that is used for performing seismic cone penetration testing (SCPT). SCPT (Robertson et al., 1986) involves making standard CPT measurements and also acquiring a single offset vertical seismic profile (VSP). The advancing cone is paused every 1 m and a seismic signal is produced by striking the end of an I-beam that is coupled to the surface by hydraulic rams connected to the cone truck. Due to the source and receiver geometry, the recorded seismic signal is dominantly an SH wave. These VSP data typically only

capture first breaks, and therefore are used to create 1D velocity profiles rather than creating VSP reflection images such as those done by Jarvis and Knight, (2000).

At the Harkins Slough pond site, we acquired 3 SCPT profiles to depths of approximately 30 m along our main seismic acquisition line (Figure 2). Figure 3 shows the results from a CPT test at location CPT2 (Figure 2). The first column is the tip resistance, the second is the friction sleeve measurement, the third is the induced pore pressure. The final column is the interpreted soil behavior type (SBT), determined using the interpretation scheme of Robertson (1990) that uses the measured tip resistance and friction ratio to generate a lithology profile. The SBT is calibrated for deltaic environments and is indicative of how a soil is behaving mechanically; it does not directly provide information about the grain size distribution. Through inspection of the CPT data, we were able to determine, from tip resistance and friction ratio, that there is a soft layer, likely a silt or clay, present in all three logs at a depth of approximately 27 m, with a thickness varying from 1 to 2 m. In addition, the large spike in the CPT pore pressure response (Figures 3 and 4), indicates this layer to be fine-grained, and relatively impermeable. (The spike occurs when the cone is pushed into an impermeable layer and the induced pore pressure cannot drain, causing pore pressure to rise far above equilibrium levels.) This impermeable layer is underlain by a very stiff layer, most likely the sand and/or gravel identified in the drillers' logs from nearby wells. At locations CPT1 and CPT3, the cone was unable to advance into this layer, whereas at CPT2 we were able to push it approximately 1 m but no further into the deeper layer. This refusal equates to approximately 30 tons of downward force produced by the CPT truck.

DESCRIPTION OF SEISMIC REFLECTION DATA

We collected SH-wave seismic data along the three lines shown in Figure 2. All data were collected with 72 live channels. For lines 1 and 3, we rolled 24 channels during acquisition for a total of 96 recording locations for each line. We recorded SH-wave data with 10-Hz horizontal geophones oriented perpendicular to the survey line. We created the SH-wave energy with sledgehammer impacts on an aluminum shear source as described by Haines (2007). With the source oriented perpendicular to the survey line, summing multiple impacts on each side of the source improves the signal-to-noise ratio, and differencing the oppositely polarized data helps to minimize non-SH energy (e.g., P waves and Rayleigh waves) while also improving the signal-to-noise ratio (Helbig and Mesdag, 1982; Stumpel et al., 1984). Line 1 was recorded with a 3-m receiver and shot spacing in an effort to characterize deeper layers and to provide longer offsets for refraction velocity analysis. Lines 2 and 3 were recorded with a 1-m receiver and shot spacing in order to better resolve shallow reflections and to better avoid any aliasing. We show only data from overlapping lines 1 and 3. Line 2 data show similar features to the line 3 data.

Representative shot gathers are shown in Figure 5, with features of interest labeled. Several clear reflections can be observed in each shot gather, from as shallow as approximately 0.06 s (R1 in Figure 5b). The deepest clear reflection arrives at approximately 0.25 s (R5), and is more evident in the line 1 gather (Figure 5a). Undesired, coherent energy is visible in both gathers. In addition to the typical

refractions and surface waves, vehicle noise from the adjacent agricultural fields may be seen, and is labeled “noise” in Figure 5a. The data from line 3 show strong dipping energy that we interpret as bounced (reflected/diffracted) surface waves; two prominent examples are identified in Figure 5b as “BSW”, and others are visible. These arrivals appear on all gathers, and originate at particular points in the shallow subsurface (presumably in the upper few meters). Data quality is uniform along line 3 and the corresponding (central) part of line 1. Relative to the generally uniform noise levels, signal strength is lower near the two ends of line 1, resulting in fewer interpretable reflections.

We combined the data from lines 1 and 3 and processed the data together using a fairly standard near-surface reflection processing flow (e.g., Baker, 1999). Our final processing flow consists of (1) muting noisy traces, (2) application of elevation statics, (3) frequency-wavenumber (f-k) filtering in the common-offset domain to minimize the diffracted surface waves, (4) top (refraction) muting, (5) correcting for normal moveout (NMO), (6) scaling by traveltime raised to a power of 1.3, (7) automatic gain control (AGC) with a centered 100-ms window, (8) common-midpoint (CMP) stacking, (9) time-variant Ormsby bandpass filtering, and (10) a second AGC also with a centered 100-ms window. Elevation static corrections were made using a velocity of 270 m/s, moving the data to a flat datum at 5.2-m depth (essentially equal to the lowest elevation along the line).

The one non-standard processing step in this flow is the common-offset-domain f-k filter, illustrated in Figure 6. The diffracted surface waves show a strongly dipping,

cross-hatched pattern in the common-offset domain (Figure 6a) and are flat in the CMP domain, leading to a strong cross-hatched pattern in the stacked section. As shown in Figure 5, these arrivals are distinct in the shot domain. They are, however, more readily separated from the signal in the common offset domain and so it is here that we perform f-k filtering in order to minimize any unwanted effects of the filter. The result of applying the filter, for one common-offset panel (offset=3 m), is shown in Figure 6b, along with the removed energy in Figure 6c. These waves can be a serious form of noise in near-surface data. Though their visual impact on the final stacked section has been significantly reduced by our simple filtering step, this noise does limit the overall data quality and would add further difficulty to any advanced processing steps that we might consider (e.g., full-waveform processing, etc). Implementation of more sophisticated (and costly) signal/noise separation techniques such as those described by Haines et al. (2007) would likely produce an improved, but still imperfect, result.

The resulting reflection section is shown in Figure 7. This is a time section, but for display and preliminary inspection purposes, a depth scale corresponding with a velocity of 350 m/s is also plotted. The reflection section shows a discontinuous reflection at approximately 0.06 seconds (R1 in Figure 5), possibly corresponding with the jump in CPT tip resistance that is observed at a depth of approximately 10 m. Deeper in the reflection section is a laterally continuous reflection at approximately 0.14 s (R3 in Figure 5). This corresponds with a depth of approximately 27 m, which is roughly the depth of the layer inferred from the CPT data (Figure 4). We interpret this reflection to be due to the impermeable layer. If this is a continuous clay layer, as is implied by seismic reflection and CPT data, the water percolating from the pond could

remain above this layer and not reach the capture zone of the recovery wells – that is, this seismic reflection section might explain the low recovery of percolated water. In this time section, the clay layer appears to be dipping, whereas the CPT data indicate that it is approximately flat. Deeper in the section, there is a strong reflection at approximately 0.18 s (R4 in Figure 5). We interpret this as corresponding to the top of the lower clay layer (shown schematically in Figure 1) that is intended to be the base of the recovery zone for this recharge pond, at a depth of approximately 50 m. This layer also appears to be dipping in the time section. Deeper still, arriving at a time of approximately 0.25 s (R5 in Figure 5), is another coherent reflector. One possible interface of origin is the base of the lower clay. Also notable in Figure 7 is the clear difference in data quality (signal strength) between the ends of the line and the center. This difference is readily apparent even when looking only at the Line 1 data (3-m spacing) and thus is not solely due to the acquisition parameters.

The first velocity model that can be considered for depth conversion is the stacking velocity model that we developed through standard velocity analysis techniques (e.g., Yilmaz, 2001) for NMO correction. Our stacking velocities correspond with interval velocities ranging from 140 to nearly 700 m/s and show rapid changes with both depth and lateral position. Additionally, the reflection arrivals from wider angles are obscured by surface wave energy and thus are difficult to interpret with certainty (Figure 5). For these reasons we have determined that this velocity model is not suitable for depth conversion.

In order to develop a second velocity model, we picked first arrival times for all traces,

neglecting those where noise made accurate picking impossible. Using the diving wave tomography algorithm that is built into the ProMAX seismic processing software, we developed a set of velocity models. Rays are traced through a gridded velocity model and updates are determined with a least-squares inversion incorporating vertical and horizontal smoothing. Our best model, judged in terms of model fit and geologic reasonableness, is shown in Figure 8. Ray coverage is dense in the upper 5 to 10 m below the ground surface, and increasingly sparse below 15 or 20 m; only the part of the model that has sufficient ray coverage to be considered reliable is shown. The model shows a zone of low velocity in the central part of the model space to a depth of approximately 5 m below the ground surface, and it shows higher velocities on the edges and at depth. Though this velocity model is not constrained to sufficient depth to allow for depth conversion of our reflection section, it does provide a sense of the upper velocity structure and it also provides the velocity that we use for elevation static corrections (270 m/s).

IMPROVED VELOCITY MODELS

Based solely on seismic data, we cannot determine the dip of the two clay layers, at approximately 30 m and approximately 50 m, presenting key questions that need to be addressed in order for these data to provide useful insights into the hydrogeologic structure affecting the operation of the recharge pond. We do, however, have cones extending to approximately 30 m that provide hard constraint on the depth of the upper clay layer and the overlying SH-wave velocities. In addition, drillers' logs from the recovery wells outside the pond area provide approximate depths for the lower clay

layer. This auxiliary information provides two different approaches that we can use to develop velocity models for our reflection section. The first relies on the standard CPT data and the drillers' logs, and the second relies on the SCPT data.

Inverting reflected and refracted arrivals to obtain a velocity model

Zelt and Smith (1992) described methods for determining velocity models to fit both reflected and refracted arrival times, using ray tracing through a model defined by velocity nodes that are specified at arbitrary locations along discrete layer boundaries. Model layers are also defined by arbitrarily located boundary nodes. Velocity can differ sharply between adjacent layers, or it can be forced to remain constant across layer boundaries. Velocity and layer boundary depth are linearly interpolated between specified nodes. The starting velocity model is updated by applying a method of damped least-squares to the linearized inversion, with the option of choosing which velocity nodes and which layer-depth nodes (if any) are allowed to change and which remain fixed. The algorithm that they describe is freely available as the research code rayinvr.

We applied the methods of Zelt and Smith (1992) to our dataset in order to develop a velocity model extending to greater depth than can be constrained with first-arrival refractions alone. We defined a model space composed of three layers. Layer 1 extends to approximately 10 m, a depth chosen based on the increase in CPT tip resistance and on seismic first break indication of a velocity increase at that depth. Layer 2 extends from the base of layer 1 to the depth of the upper clay layer as seen in the CPT logs, approximately 28 m. Layer 3 extends to the depth of the top of the lower

clay layer as seen in drillers' logs from nearby wells, approximately 37 m. Velocity is allowed to differ sharply across layer boundaries, in keeping with our understanding of the site geology. Thus, the layer boundaries are evident in the final velocity model (Figure 9) as the locations of sharp velocity increase at approximately 10-m and 28-m depths. The layer boundary depths are held fixed during inversion because we consider them (particularly the base of layers 2 and 3) to be known. Velocity is specified at nodes along the top and bottom of each layer. These nodes are spaced at 25-m intervals along the top and bottom of layer 1 and along the top of layer 2. For the bottom of layer 2, velocity nodes are specified at 25-m intervals between lateral positions 75 m to 225 m, and at 50 m outside of that central zone (due to ray coverage limitations). Velocity for layer 3 is defined only at one node each for the top and bottom (that is, the layer velocity is laterally homogeneous), because we lack exact knowledge of the layer depth, and because the reflection arrival times for the lower clay are uncertain in many places.

Our model is constrained by three sets of arrival time data: the refraction first arrivals, reflected arrivals from the upper clay (corresponding with the bottom of layer 2), and reflected arrivals from the lower clay (corresponding with the bottom of layer 3). We picked reflection arrivals on a true-time, zero-offset stacked section (static corrections were not applied), while also looking carefully at the reflected arrivals in the shot and CDP domains to improve pick certainty. Although it would have been preferable to base our model on arrivals picked at broad offsets in the shot domain, data quality and lack of clear moveout trends necessitated that we pick only a single reflection arrival time for each lateral position along the line (zero offset reflections) in order to avoid

erroneous or highly uncertain picks.

Starting with a 1-D (laterally homogeneous) velocity model and working our way from shallower to deeper layers, we used procedure of inversion and forward modeling to determine a set of velocity models with various parameter choices. Our preferred model (in terms of consistency with other models, fit of the model to the data, and geologic reasonableness) is shown in Figure 9.

Inverting SCPT arrivals to obtain a velocity model with error estimates

The SCPT data acquired at this site provide an alternate means of obtaining a velocity model of the subsurface. The standard procedure for processing SCPT data (Roberston et al., 1986) assumes perfect travel time picking and straight ray propagation between source and receiver. We believe that a better approach is to incorporate errors in traveltimes and in raypath estimates and then to solve the system using an integrated forward operator (Lizarralde and Swift, 1999) and a Bayesian inversion scheme (Malinverno and Briggs, 2004; Tarantola, 1987). We use cross-correlation with the shallowest trace as a reference trace to obtain traveltimes for all permutations of the traces; assuming Gaussian statistics, we use the standard deviation of these estimates to obtain traveltimes errors. Velocity is determined through a Bayesian framework so that traveltimes errors are accounted for in the resulting velocity model. This approach provides shear wave velocity along with estimates of the error in each layer of the velocity model.

Our resulting SCPT velocity columns are shown in Figure 10, along with the

corresponding 95% confidence intervals. These results demonstrate the need for incorporating error estimates when using SCPT data, as the confidence intervals for several of the model parameters are quite wide. For comparison, the corresponding velocity columns extracted from the reflection/refraction model are also shown; the generally good fit between results from these two independent velocity estimates is reassuring. Figure 9b shows the 2-D velocity model resulting from linear interpolation between the 1-D velocity columns and extrapolation outside CPT's 1 and 3.

Depth-converting our reflection section with our new velocity models

Depth conversions for our reflection section, corresponding with our two velocity models, are shown in Figure 11. The two conversions are similar, but the SCPT-based conversion maps the reflections approximately two meters deeper (Figure 11b) in the central part of the model space, down to the reflection from the upper clay (at about 27 m in Figure 11a). Below this depth, the SCPT conversion plots reflections considerably shallower (and yields less stretch), a result of extrapolating slow velocities below the deepest measurements. The reflection/refraction velocity model (Figure 9a) includes velocity estimates to the lower clay at 37-m depth and thus better places that reflection. The discrepancy between the depths of the two clays is not unexpected; the reflection/refraction model includes robust velocity estimates to greater depth than the SCPT model. The good fit of both main reflectors in the reflection/refraction conversion is also to be expected, in that the model was specifically designed to correctly convert these reflections. More surprising is the apparent error in the SCPT velocities, particularly in the middle part of the image (around CPT2 and to a lesser degree near CPT3) where the two velocity models differ. The velocity models and

conversions are similar nearer to CPT1.

DISCUSSION

With the goal of improving the understanding of the subsurface structure beneath the pond, we focused on using a multimodal approach to acquiring a robust velocity model, which would yield an accurate seismic reflection section. The two velocity models that we developed are based on different surveys with different perceived reliabilities and they agree well at depths below 10 m (Figure 11). This comparison indicates that the two models are fairly robust. This is further supported by the similarity between the reflection/refraction model (Figure 9a) and the diving-wave refraction model (Figure 8); the two were created through very different algorithms. We consider the SCPT velocity model to be more appropriate for small (meter) scale interpretation or property estimation, particularly because velocity is estimated within a known confidence interval. If we desired finer spatial resolution (a smaller support volume) we could simply make SCPT measurements at a finer depth interval. Though the reflection/refraction model provides a good depth conversion without explicitly requiring SCPT or VSP data it is important to note that knowledge of interface depth from CPT or borehole information is essential to the algorithm as we implemented it. An alternative approach would be to exploit reflection curvature to constrain velocity without requiring a priori depth information; however, surface-wave obscurement of long-offset reflection energy precludes such an approach with our dataset.

The divergence of the two models in the upper few meters, especially at CPTs 2 and 3,

is unexpected as both models should have particularly good resolution and accuracy at shallow depths. Low shear wave velocities in the refraction/reflection-derived model indicate that the sand in the bottom of the pond is very loosely packed whereas the SCPT measurements suggest that the sand is considerably stiffer. We believe that this is not an error in either measurement, but that it in fact reflects the stress influence of the 30-ton cone truck on the velocity of the underlying sediments. Because these are clean, dry sands, the soil will respond to the stress increase with negligible time lag. For a set of Newmark stress analyses (Newmark, 1942), based on reasonable values for the footprint and mass distribution of the cone truck, we find a range of possible values for the impact of the truck on total vertical stress in the upper few meters; these allow us to estimate the truck's impact on velocity. For SCPT measurements made at depths between 2 and 5 m, the presence of the truck would be approximately equivalent to an extra 1 to 1.5 m of overburden. Another way of looking at this is that the SCPT velocity profile can be shifted down by approximately 1.25 m, to an "equivalent" depth in terms of in situ stress conditions at the time of measurement. As can be seen in Figure 10, a vertical shift of 1.25 m would bring the velocity estimates for CPT's 2 and 3 into better agreement with the reflection/refraction velocity model. At CPT1, the two velocity estimates (Figure 10) show a good fit without shifting (though a 1.25-m shift would have only minimal impact on this fit). We suggest that the apparently minimal impact of the cone truck mass at this location is due to the sediment at CPT1 (on the shoulder of the pond) being considerably stiffer and less sensitive to additional overburden than the sediment in the pond bottom. This stiffness differential is indicated by the higher S-wave velocity measured in that location by all measurement methods and by the CPT tip resistance data (significantly higher for CPT 1 than for

CPTs 2 and 3). Although this simple stress analysis supports our interpretation regarding the cone truck mass, it neglects many aspects of the system that may be important (e.g., plastic deformation due to loading by the cone truck); a more definitive interpretation will likely require additional testing and/or modeling of the stress influence.

CONCLUSIONS

This study has demonstrated the use of shear-wave reflection, CPT, and SCPT data to develop a model of the hydrogeologic structure of the region underlying the Harkins Slough recharge pond. We combined information from the three types of data to identify a clay layer at the site that is potentially blocking the movement of much of the percolating water; if correct, this interpretation can explain the low recovery rate of water in the capture zone of the recovery wells. We have also identified the cone truck's "overburden" effect on the shear wave velocity of soft sands in the upper few meters; this interpretation has implications for the use of SCPT-derived velocities at sites with similarly soft sediments. Our velocity model comparison emphasizes the need for independent methods if one is to glean useful information from seismic reflection images in areas of complex velocity heterogeneity. We conclude that the acquisition of seismic and CPT data can provide valuable information about subsurface structure that can assist in planning the design and operation of a recharge pond.

ACKNOWLEDGMENTS

We are grateful to Brian Lockwood, Mary Bannister and others from the Pajaro Valley Water Management Agency and to Jonathan Lear of Balance Hydrologics for their assistance and cooperation with this work. We thank Bob Clapp of Stanford University and Olav Lindtjorn and Chung-Chi Shih from Schlumberger for helpful discussions regarding velocity modeling algorithms. We also thank Vanessa Mitchell and Elliot Grunewald for their participation in the seismic data collection. This research was supported by funding to R. Knight from Schlumberger Water Services. References to any specific commercial product, process, or service by trade name, trademark, manufacturer, or otherwise does not necessarily constitute or imply its endorsement, recommendation, or favoring by the United States Government or any agency thereof.

REFERENCES

- Baker G. S. 1999. Processing near-surface seismic-reflection data: A primer. Society of Exploration Geophysics.
- Bradford J. H., Liberty L., Lyle M., Clement W. and Hess S. 2006. Imaging complex structure in shallow seismic-reflection data using prestack depth migration. *Geophysics* 71, B175-B181.
- Brouwer J and Helbig K. 1998. Shallow high-resolution reflection seismics. Elsevier.
- Bouwer H. 2002. Artificial recharge of groundwater: hydrogeology and engineering. *Hydrogeology Journal* 10, 121-142.
- Campanella R. G. and Robertson P. K. 1984. A seismic cone penetrometer to measure engineering properties of soil. 54th Annual Society of Exploration Geophysics Meeting, Atlanta, Expanded Abstracts, 138-141.

- Campanella R. G. and Weemees I. 1990. Development and use of an electrical resistivity cone for groundwater contamination studies. *Canadian Geotechnical Journal* 27, 557-567.
- Carr B. J., Hajnal Z. and Prugger A. 1998. Shear-wave studies in glacial till. *Geophysics* 63, 1273-1284.
- Daniel C. R., Giacheti H. L., Howie J. A. and Campanella R. G. 1999. Resistivity piezocone: Data interpretation and potential applications. XI Panamerican Conference on Soil Mechanics and Geotechnical Engineering. Foz do Iguassu, Brazil. Conference Volume 1, 361-368.
- Ghose R. and Goudswaard J. 2004. Integrating S-wave seismic reflection data and cone-penetrometer-test data using a multiangle multiscale approach. *Geophysics* 69, 440-459.
- Haines S. S. 2007. A Hammer-impact, aluminum, shear-wave seismic source. U.S. Geological Survey Open-File Report 2007-1406.
<http://pubs.usgs.gov/of/2007/1406/>.
- Haines, S., Guitton, A., Biondi, B., 2007, Seismoelectric data processing for surface surveys of shallow targets, *Geophysics*, 72, no 2, p G1-G8, doi 10.1190/1.2424542.
- Hasbrouck W.P. 1991. Four shallow-depth, shear-wave feasibility studies. *Geophysics* 56, 1875-1885.
- Helbig K. and Mesdag C. S. 1982. The potential of shear-wave observations. *Geophysical Prospecting* 30, 413-431.

- Hunter J. A., Pullan S. E., Burns R. A., Gagne R. M. and Good R. L. 1984. Shallow seismic reflection mapping of the overburden-bedrock interface with the engineering seismograph – Some simple techniques. *Geophysics* 49, 1381-1385.
- Jarvis K. D. and Knight R. 2000. Near-surface VSP measurements using the seismic cone penetrometer. *Geophysics* 65, 1048-1056.
- Jarvis K. D. and Knight R. J. 2002. Aquifer heterogeneity from SH-wave seismic impedance inversion. *Geophysics* 67, 1548-1557.
- Lizarralde D. and Swift S. 1999. Smooth inversion of VSP travelttime data. *Geophysics* 64, 659–661.
- Malinverno A. and Briggs V. A. 2004. Expanded uncertainty quantification in inverse problems: Hierarchical Bayes and empirical Bayes. *Geophysics* 69, 1005-1016.
- Martí D., Carbonell R., Flecha I., Palomeras I., Font-Capó J., Vázquez-Suñé E. and Pérez-Estaún A. 2008. High-resolution seismic characterization in an urban area: Subway tunnel construction in Barcelona, Spain. *Geophysics* 73, B41-B50.
- Newmark N.M. 1942. Influence charts for computation of stresses in elastic soils. University of Illinois Experiment Station. Bulletin No. 338.
- Palmer D. 1981. An introduction to the generalized reciprocal method of seismic refraction interpretation. *Geophysics* 46, 1508-1518.
- Pugin A., Larson T., Sargent S., McBride J. and Bexfield C. 2004. Near-surface mapping using SH-wave and P-wave seismic landstreamer data acquisition in Illinois, U.S. *The Leading Edge* 23, 677-682.
- Robertson P. K., Campanella R. G., Gillespie D. and Rice A. 1986. Seismic CPT to measure in situ shear wave velocity. *Journal of Geotechnical Engineering* 171, 791-803.

- Robertson P.K. 1990. Soil Classification using the cone penetration test. *Canadian Geotechnical Journal* 27, 151-158.
- Steeple D.W. and Miller R.D. 1990. Seismic reflection methods applied to engineering, environmental and groundwater problems. In: *Geotechnical and Environmental Geophysics*, Vol. 1(ed. S. A. Ward), pp 1-29. Society of Exploration Geophysics.
- Steeple D.W. and Miller R.D. 1998. Avoiding pitfalls in shallow seismic reflection surveys. *Geophysics* 63, 1213-1224.
- Stork C. and Clayton R. W. 1991. Linear aspects of topographic velocity analysis. *Geophysics* 56, 483-495.
- Stumpel H., Kahler S., Meissner R. and Milkereit B. 1984. The use of seismic shear waves and compressional waves for lithologic problems of shallow sediments. *Geophysical Prospecting* 32, 662-675.
- Tarantola A. 1987. *Inverse problem theory: Methods for data fitting and model parameter estimation*. Elsevier.
- Woolery E. W., Street R. L., Wang Z., Harris J. B. 1993. Near-surface deformation in the New Madrid seismic zone as imaged by high resolution SH-wave seismic methods. *Geophysical Research Letters* 20, 1615-1618.
- Yilmaz O. 2001. *Seismic Data Analysis*. Society of Exploration Geophysics.
- Zelt C. A. and Smith R. B. 1992. Seismic travelttime inversion for 2-D crustal velocity structure. *Geophysical Journal International* 108, 16-34.
- Zelt C. A., Azaria A. and Levander A. 2006. 3D seismic refraction travelttime tomography at a groundwater contamination site. *Geophysics* 71, H67-H78.

List of Figures

Figure 1. Cross section schematic of the Harkins Slough pond site, Pajaro Valley, California.

Figure 2. Plan-view schematic of the Harkins Slough pond site. The solid line shows the recharge pond boundary, and the dashed line marks the inner, deeper, part of the pond. Seismic line 3 overlaps with the central part of line 1.

Figure 3. Cone penetrometer (CPT) measurements for location CPT2, where the ground surface is at approximately 4 m below our datum. Measurements are described in the text.

Figure 4. Induced pore pressure measurements for all three cones. Induced pore pressure is generally low except for the spike observed on all three cones at approximately 28-m depth.

Figure 5. Representative shear-wave shot gathers for (a) line 1 and (b) line 3. Selected reflection arrivals are labeled R1 through R5. Vehicle noise from adjacent agricultural fields is labeled in (a) as “noise”. Examples of bounced surface waves (dipping linear features) are labeled in (b) as BSW. Display processing for this figure consists of 10 to 500 Hz bandpass filter and automatic gain control with a 62.5-ms centered window.

Figure 6. Common-offset-domain plots for offset=3 m showing a) unfiltered data, b) result after fk filtering, and c) energy removed by fk filter. All data are plotted with the same clip level and with gain equal to time raised to the 1.7 power.

Figure 7. SH-wave reflection section, in time. A rough-estimate depth conversion is also shown for preliminary interpretation.

Figure 8. SH-wave velocity model from turning-wave refraction analysis.

Figure 9. SH-wave velocity models from (a) reflection/refraction inversion and (b) SCPT arrival inversion.

Figure 10. Velocity columns for the three SCPT studies in dark grey and the 95% confidence interval indicated by the light grey zone. Arrows and numbers indicate maximum value for confidence interval where this value is off scale. Corresponding velocity columns extracted from the reflection/refraction model are plotted as black lines.

Figure 11. Depth-converted reflection sections. a) Converted with the reflection/refraction velocity model. b) Converted with the SCPT velocity model. c) same conversion as in (a), with interpretations overlain.

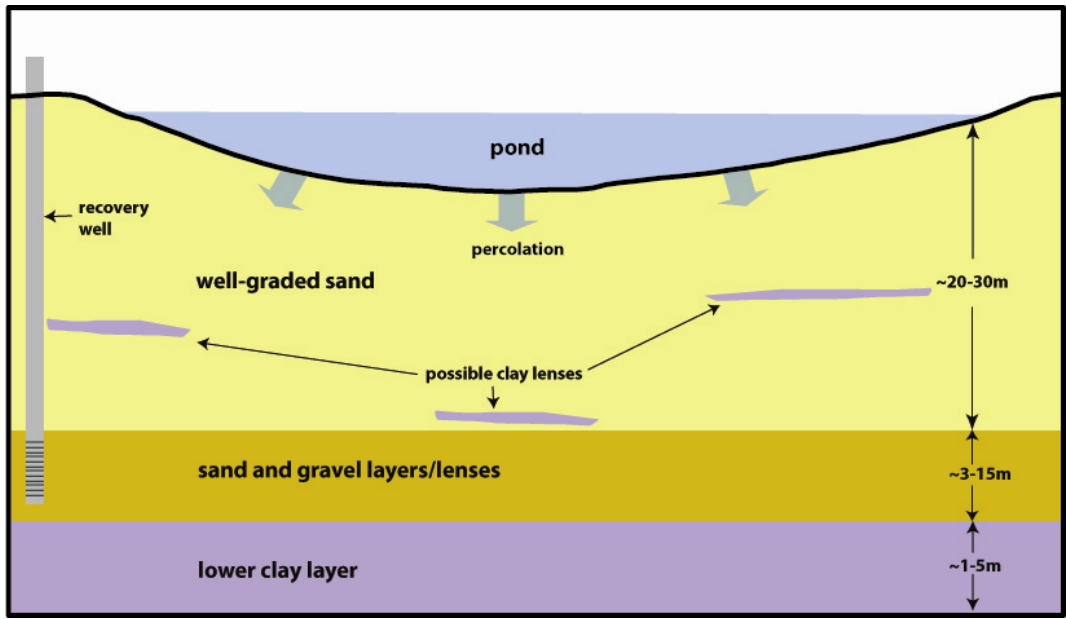


Figure 1. Cross section schematic of the Harkins Slough pond site, Pajaro Valley, California.

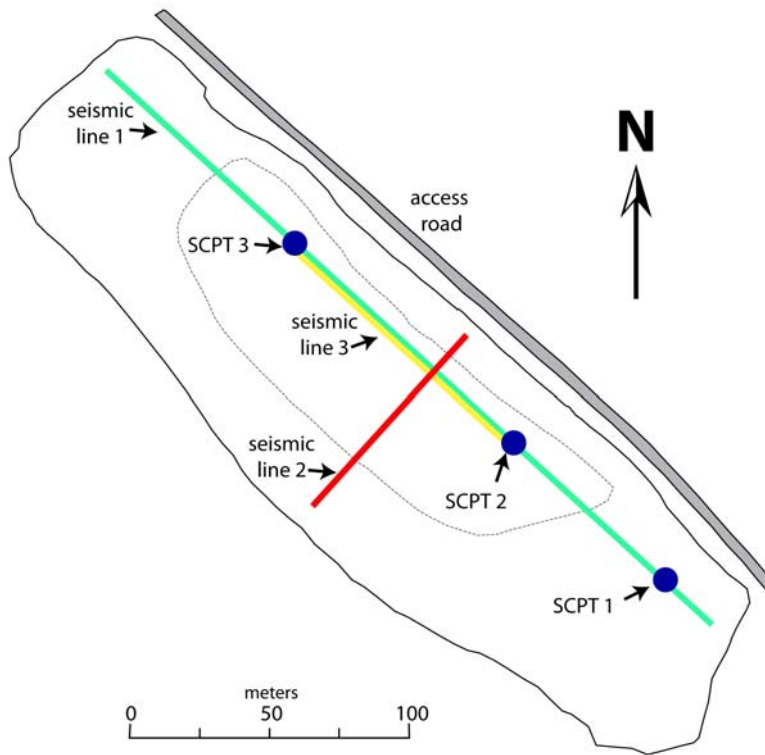


Figure 2. Plan-view schematic of the Harkins Slough pond site. The solid line shows the recharge pond boundary, and the dashed line marks the inner, deeper, part of the pond. Seismic line 3 overlaps with the central part of line 1.

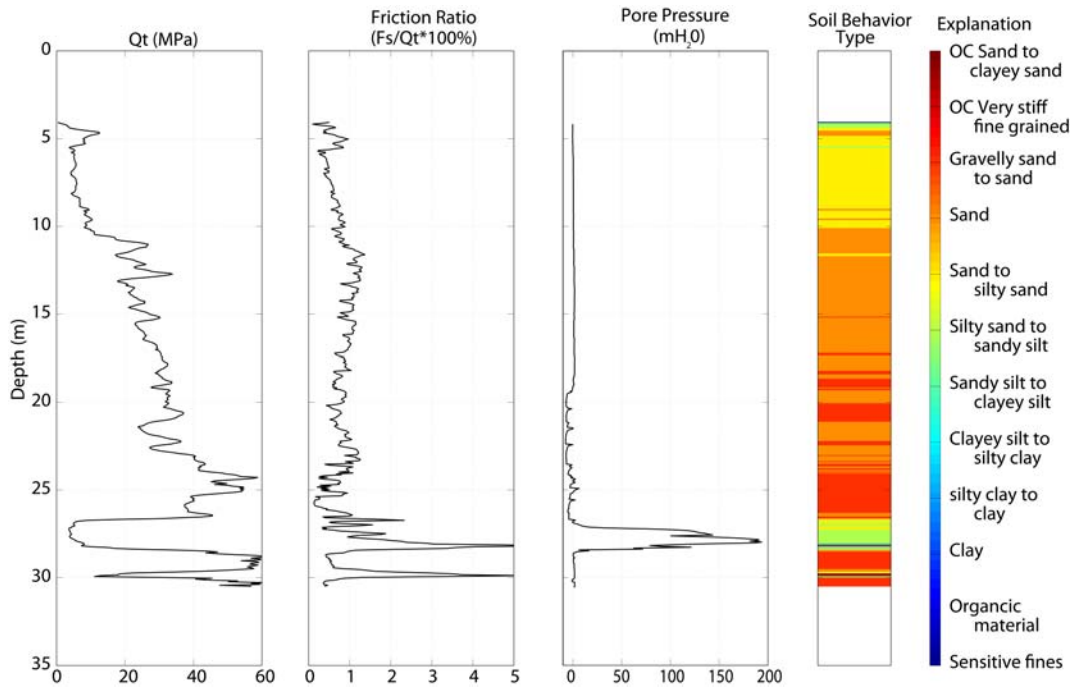


Figure 3. Cone penetrometer (CPT) measurements for location CPT2, where the ground surface is at approximately 4 m below our datum. Measurements are described in the text.

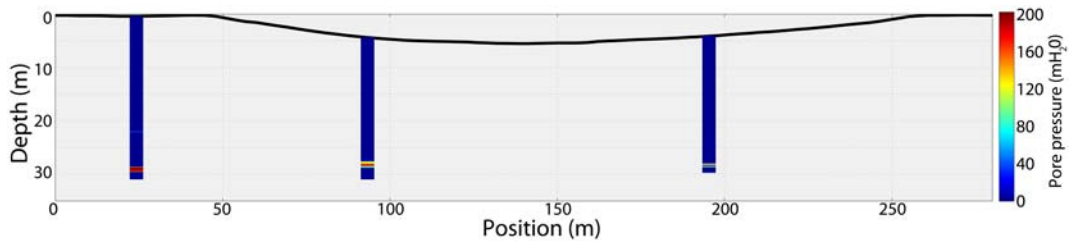


Figure 4. Induced pore pressure measurements for all three cones. Induced pore pressure is generally low except for the spike observed on all three cones at approximately 28 m depth.

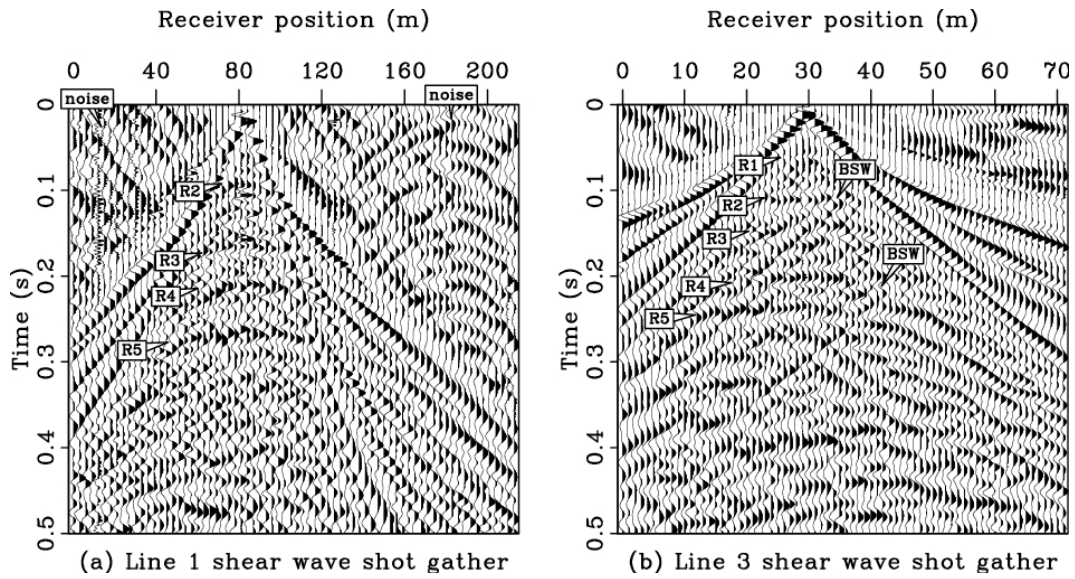


Figure 5. Representative shear-wave shot gathers for (a) line 1 and (b) line 3. Selected reflection arrivals are labeled R1 through R5. Vehicle noise from adjacent agricultural fields is labeled in (a) as “noise”. Examples of bounced surface waves (dipping linear features) are labeled in (b) as BSW. Display processing consists of 10 to 500 Hz bandpass filter and automatic gain control with a 62.5 ms centered window.

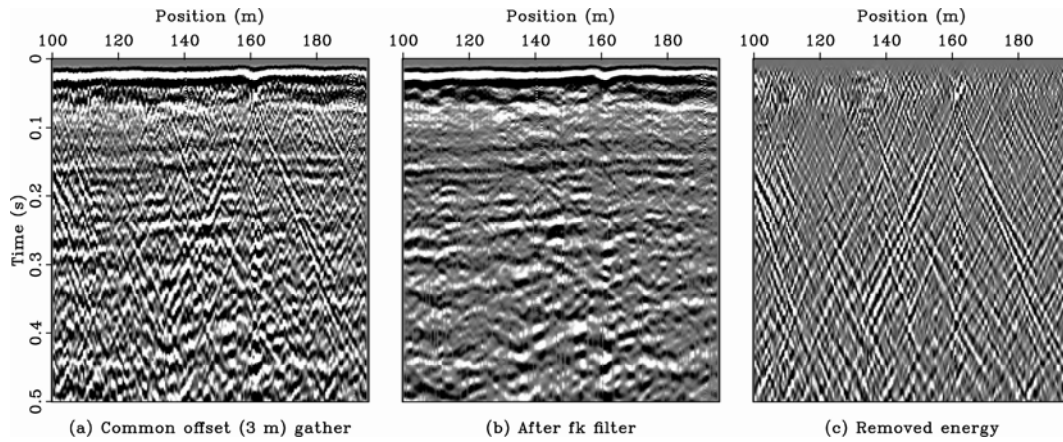


Figure 6. Common-offset-domain plots for offset=3 m showing a) unfiltered data, b) result after fk filtering, and c) energy removed by fk filter. All data are plotted with the same clip level and with gain equal to time raised to the 1.7 power.

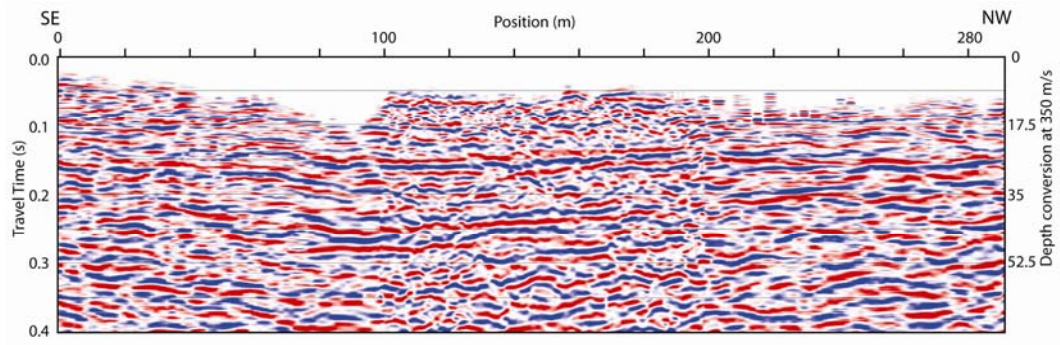


Figure 7. SH-wave reflection section, in time. A rough-estimate depth conversion is also shown for preliminary interpretation.

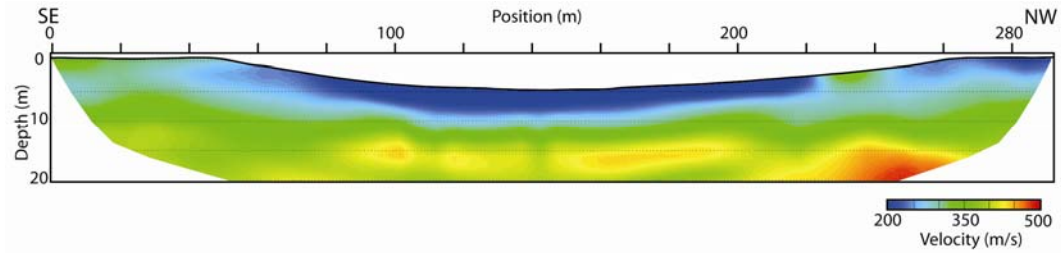


Figure 8. SH-wave velocity model from turning-wave refraction analysis.

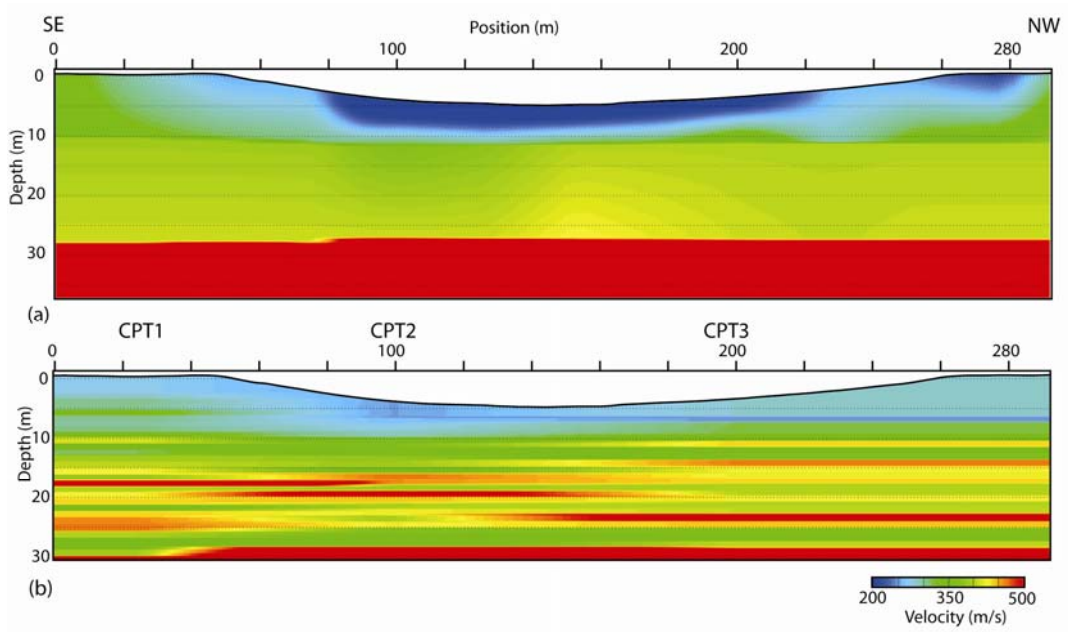


Figure 9. SH-wave velocity models from (a) reflection/refraction inversion and (b) SCPT arrival inversion.

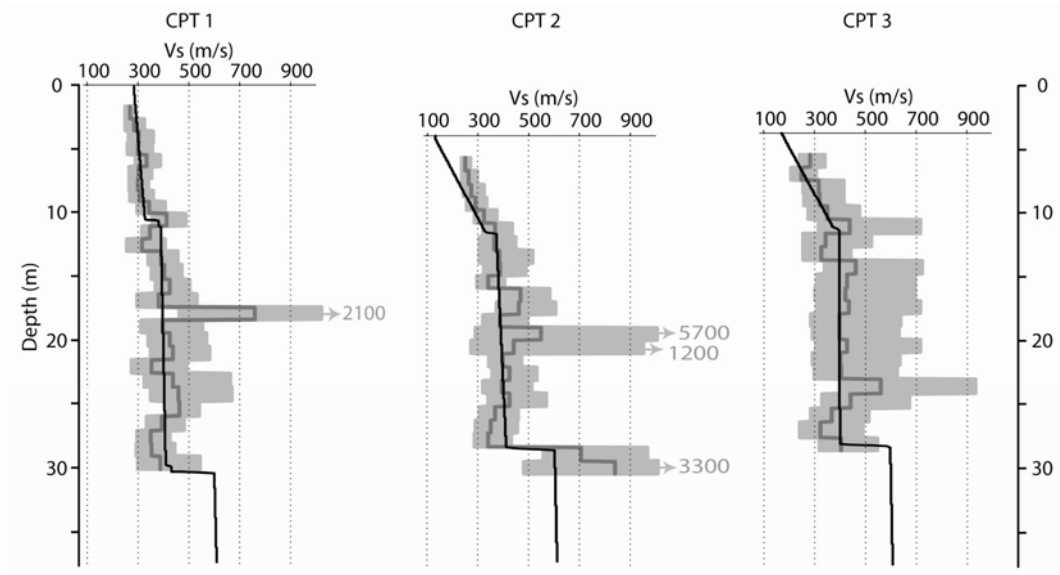
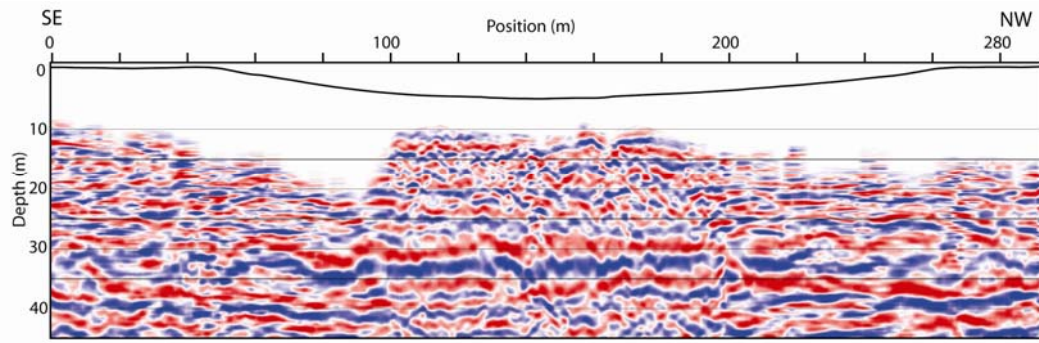
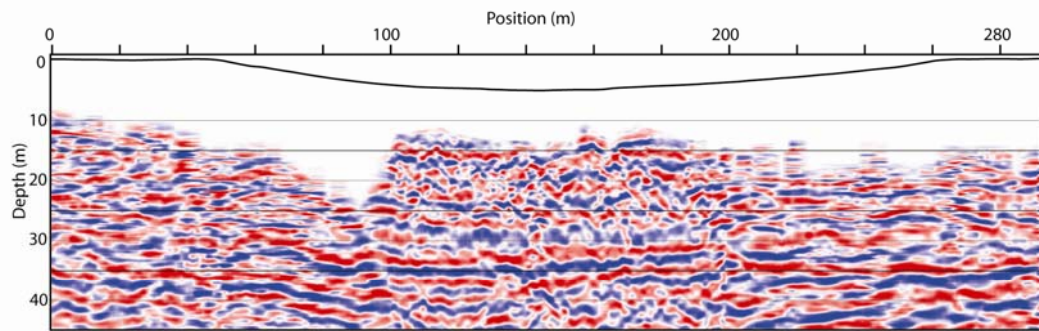


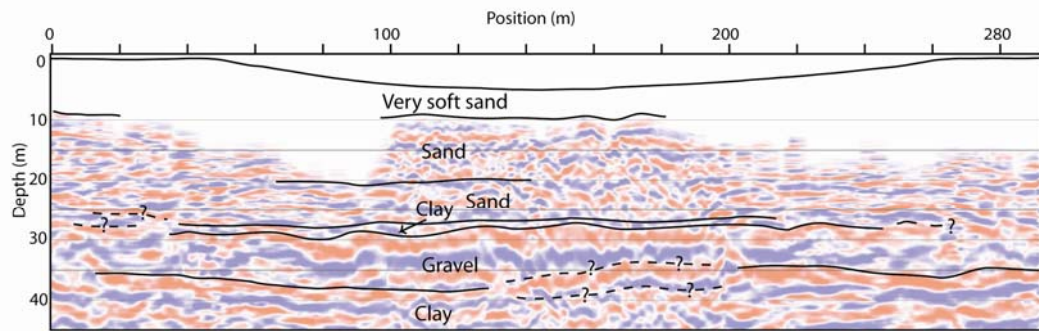
Figure 10. Velocity columns for the three SCPT studies in dark grey and the 95% confidence interval indicated by the light grey zone. Arrows and numbers indicate maximum value for confidence interval where this value is off-scale. Corresponding velocity columns extracted from the reflection/refraction model are plotted as black lines.



a) Depth-converted using reflection/refraction velocity model



b) Depth-converted using interpolated cone VSP velocity model



c) Interpreted reflection section

Figure 11. Depth-converted reflection sections. a) Converted with the reflection/refraction velocity model. b) Converted with the SCPT velocity model. c) same conversion as in (a), with interpretations overlain.